NASA-CR-205365

AIAA 94-0741
Design of a High Thermal Gradient Bridgman Furnace

J. E. LeCroy and D. P. Popok
Teledyne Brown Engineering
Huntsville, Alabama

32nd Aerospace Sciences Meeting & Exhibit
January 10-13, 1994 / Reno, NV

DESIGN OF A HIGH THERMAL GRADIENT BRIDGMAN FURNACE

J. E. LeCroy* and D. P. Popok
Teledyne Brown Engineering
Huntsville, AL USA

Abstract

The Advanced Automated Directional Solidification Furnace (AADSF) is a Bridgman-Stockbarger microgravity processing facility, designed and manifested to first fly aboard the second United States Microgravity Payload (USMP-2) Space Shuttle mission. The AADSF was principally designed to produce high axial thermal gradients, and is particularly suitable for metals solidification experiments, including non-dilute alloys. To accommodate a wider range of experimental conditions, the AADSF is equipped with a reconfigurable gradient zone. The overall design of the AADSF and the relationship between gradient zone design and furnace performance are described. Parametric thermal analysis was performed and used to select gradient zone design features that fulfill the high thermal gradient requirements of the USMP-2 experiment. The thermal model and analytical procedure, and parametric results leading to the first flight gradient zone configuration, are presented. Performance for the USMP-2 flight experiment is also predicted, and analysis results are compared to test data.

Introduction

The NASA Marshall Space Flight Center conceived and funded development for the Advanced Automated Directional Solidification Furnace (AADSF), which will fly on the second United States Microgravity Payload (USMP-2) mission in early 1994. The AADSF is a Bridgman-Stockbarger crystal growth furnace designed to operate in a microgravity environment on orbit. Manifested on several future USMP science missions, the AADSF flies on a multi-purpose experiment support structure (MPESS) in the space shuttle payload bay. For the first flight experiment, the AADSF is configured to maximize the axial temperature gradient at the crystal growth interface. This paper describes the engineering process used to select the gradient zone design features that enable the AADSF to produce the high thermal gradients needed by the USMP-2 experiment.

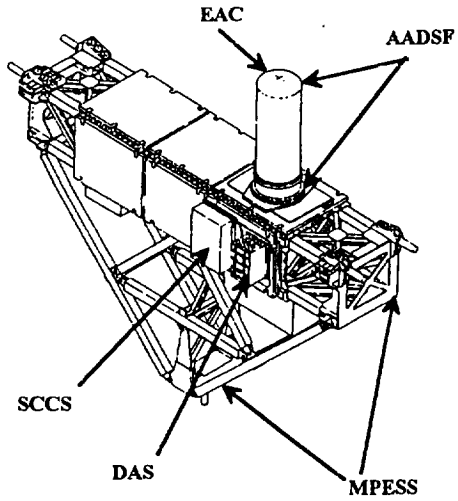

Figure 1: AADSF System Flight Configuration

The AADSF system consists of three major components, the furnace assembly, the Data Acquisition System computer (DAS), and the Signal Conditioning and Control System (SCCS). Figure 1 depicts the AADSF flight elements mounted on the MPESS. A sealed experiment apparatus container (EAC) provides an inert gas atmosphere for the three zone Bridgman-Stockbarger furnace and the sample translation and experiment telemetry subsystems. The DAS collects analog data for downlink during processing. The SCCS conditions sample and control thermocouple signals, stores experiment timelines, and accomplishes closed-loop control of the individual furnace heaters and the sample translation system.

Furnace Design

The AADSF can ultimately attain hot zone temperatures of up to 1600°C. However, for the first two flights, heat extraction plate and control thermocouple material choices limit the maximum operational temperature to 1150°C in the hot zone and 850°C in the cold zone. The furnace bore diameter permits processing with sample diameters up to 20 mm. The furnace includes a 250 mm long isothermal hot zone, and a 100

*Branch Manager, Space Programs Division
Member AIAA

mm cold zone. The system accommodates sample translations up to 240 mm. The ability to change insulation and heat extraction plate thickness and material makes the gradient zone reconfigurable [1]. Changing the gradient zone adapts the furnace to different experimenter requirements. Figure 2 shows a section view of the furnace.

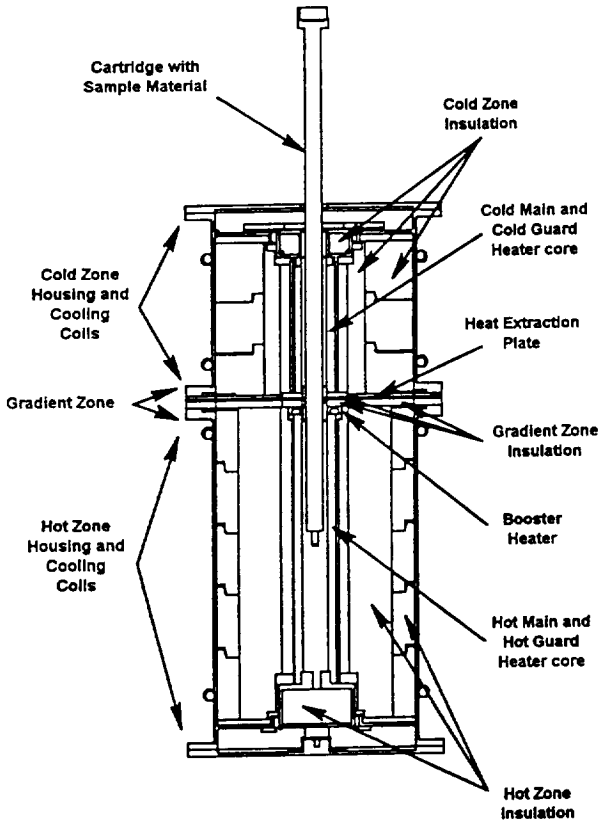

Figure 2: AADSF Cross Sectional View

To produce high temperature gradients within a sample, heat transfer across the gradient zone into the cold zone is minimized. The heat extraction plate accomplishes this by conducting heat from the hot zone to the furnace cooling system before it can reach the cold zone. Low thermal conductivity gradient zone insulation further isolates the cold zone from the hot zone. For the USMP-2 mission, the engineering performance specification required that the furnace produce temperature gradients of 100°C/cm in an instrumented quartz rod with the hot zone operating at 1100°C. This design criterion ensured sufficient temperature and gradient performance for the planned first flight experiment, with anticipated hot and cold zone temperatures near 850°C and 350°C, respectively.

Unlike a conventional two-zone Bridgman furnace, the AADSF has a booster heater at the interface between the hot zone and the gradient zone. This independently controlled heater maintains hot zone isothermality near the gradient zone. Without the booster heater, heat transfer from the hot zone to the heat extraction plate would cause furnace bore temperatures to decrease near the gradient zone, thereby degrading isothermality. The booster heater reinforces the hot main heater in this local region, improving hot zone isothermality and increasing the axial thermal gradients produced within the sample.

Crystal growth in the AADSF occurs with the translation of the sample from the hot end of the furnace through the gradient zone, where directional solidification occurs. The translation system pulls the sample through the gradient zone at controlled rates between 0.5 and 50 mm/hour. The translation rate is selected by the experimenter, based on the expected crystal growth parameters, and may be changed during processing without significantly disturbing the thermal performance of the furnace.

Experiment Design

The first flight experiment using the AADSF will be "Growth of Solid Solution Crystals - HgCdTe" aboard the USMP-2 Space Shuttle flight. The principal investigator for this experiment is Dr. S. L. Lehoczky, with co-investigators Dr. F. R. Szofran and Dr. D. C. Gillies, all of the NASA Marshall Space Flight Center.

For the USMP-2 experiment the AADSF system will process directional solidification of $Hg_{1-x}Cd_xTe$ crystals under microgravity and high thermal gradient conditions. This material behaves as a nondilute alloy of HgTe and CdTe. Under normal earth gravity conditions, this material resists compositionally uniform growth by the Bridgman-Stockbarger method. As the material solidifies, CdTe is preferentially incorporated into the crystal, and the liquid sample becomes enriched with denser HgTe near the solidification interface. Under normal earth gravity conditions, the vertical Bridgman method results in increased HgTe enrichment near the crystal/melt interface, because nondilute alloy components tend to separate due to density differences. Under microgravity conditions, diffusion becomes the only significant mechanism for HgTe enrichment in the melt, and density stratification should be nearly nonexistent, hence improving the compositional uniformity of the crystal.

The nondilute nature of $Hg_{1-x}Cd_xTe$ also drives the high gradient requirement of the USMP-2

experiment. High temperature gradients within the sample result in better control of the crystal-melt interface. High axial gradients tend to flatten the shape of the solidification interface. Also, constitutional supercooling, a problem that can result in polycrystalline directional solidification of nondilute alloys, is avoided by sufficiently high thermal gradients coupled with sufficiently low growth rates. Compositional variations in the liquid sample also cause variations in the solidification temperature during the crystal growth process. Such solidification temperature variations cause axial displacement of the interface, and high temperature gradients minimize this displacement [2].

Gradient Zone Design Options

Design options for the AADSF gradient zone included: (1) gradient zone material and thickness, and (2) heat extraction plate material and thickness. Table 1 lists properties for the candidate gradient zone materials. The USMP-2 experimenter preferred the shortest possible gradient zone, commensurate with achieving hot and cold zone temperature control at 850°C and 350°C, respectively. Based on this requirement and early analysis, zone insulation thicknesses of 7.6 mm and 4.4 mm were selected to separate the heat extraction plate from the hot zone and cold zone heater cores, respectively. In addition to the insulation components, the gradient zone also includes a 0.5 mm thick washer separating the cold zone heater core and gradient zone insulation, and the heat extraction plate. Figure 3 depicts the details of the gradient zone design.

Material	Density (g/cm^3)	Thermal Conductivity (at 1000°C) (W/m-°C)	Specific Heat (at 1000°C) (J/kg-°C)	Maximum Use Temperature (°C)
Gradient Zone Insulation Material Candidates				
FBD™ fibrous zirconia	1.4	0.33 (ave)	657	2,200
AL-30™ fibrous alumina	0.5	0.2	1,050	1,540
ZAL-45™ fibrous alumina	0.7	0.3	1,050	1,650
Alumina (99.5% dense)	3.9	6.0	1,230	2,050
Heat Extraction Plate Material Candidates				
Platinum	21.5	84	159	1,600
Inconel 718	8.2	27	712	1,100

(FBD, AL-30, and ZAL-45 are trademarks of Zircar Products Inc.)

Table 1 - Properties of Gradient Zone Insulation and Heat Extraction Plate Material Candidates

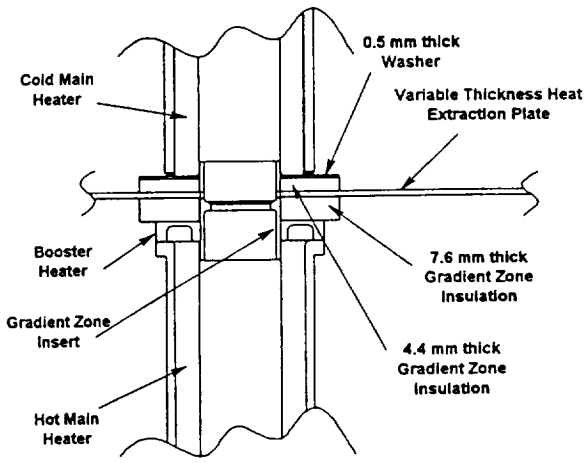

Figure 3: AADSF Gradient Zone Detail

With the thicknesses defined, gradient zone insulation material remained to be selected. Candidate gradient zone insulation materials included several low density ceramic fiber insulations and dense alumina. Pure alumina and alumina/zirconia blends were the principal candidate fibrous insulation materials. Potential silica contamination of platinum alloy control thermocouples eliminated silica based materials as gradient zone insulation candidates.

The heat extraction plate material and thickness comprised the second option for maximizing the AADSF gradient capability for the USMP-2 experiment. Several factors influenced the heat extraction plate design. Since the heat extraction plate conducts heat from the hot zone to the cooling system, the plate must withstand the thermal stresses induced by large radial temperature gradients. Radial slots were incorporated into the plate design to reduce thermal stresses induced by radial temperature gradients. The need to accommodate axial thermal expansion of the cold zone heater core limited the allowable flexural stiffness of the heat extraction plate. This low stiffness requirement led to a multi-layered plate design, which provides the necessary flexibility without sacrificing the radial thermal conductance needed to produce high gradients.

Both upper and lower bounds exist on the heat extraction plate conductance. Gradient performance requirements define the lower bound, and booster heater power limits define the upper thermal conductance

bound. Large plate conductances could degrade hot zone isothermality by loading the booster heater beyond its power limits. The relationship between the heat extraction plate and booster heater limits depends on the thermal conductance between the plate and booster heater, thus coupling the heat extraction plate and gradient zone insulation configurations to each other.

Thermal Modeling and Analysis

During development of the AADSF, several thermal models of the furnace were developed and used as design tools. The majority of the design supporting analysis was performed with an axisymmetric steady-state model of the furnace. This model was used to evaluate gradient zone configurations to ensure conformance to design specifications and mission science goals. Also, the model provided estimated heater power requirements to support sizing of the heaters, and determined component temperature distributions to support thermoelastic stress analysis. The model was also used to predict furnace performance and sample thermal profiles for the USMP-2 crystal growth experiment.

The AADSF thermal model is based on the finite difference method, and was developed for solution with the Systems Improved Numeric Differencing Analyzer (SINDA/G™) thermal solver. The SINDA thermal resistance-capacitance network was developed with PATRAN™. Although PATRAN™ is primarily a finite element mesh generator, the finite difference SINDA model was created by assigning lumped mass thermal nodes to each of the finite element centroids.

Thermal modeling goals drove the choice of analysis methods and tools. The high degree of flexibility that can be built into a SINDA model led to its selection as the thermal solver. The need to perform parametric design studies necessitated a flexible thermal model permitting efficient specification of material properties (heat extraction plate and gradient zone insulation) and some component dimensions (heat extraction plate thickness), without repetitive preprocessing. In addition to meeting these needs, the PC based version of SINDA provided an additional benefit. Once compiled, PC-SINDA models are portable and may be executed on any PC having a compatible processor. The resulting model can be made available to the Principal Investigator, and permits running simultaneous simulations on multiple PCs.

A computer aided design (CAD) program was used to develop an idealized cross sectional diagram of the furnace. From preliminary thermal analysis, the gradient zone thickness for the USMP-2 experiment was selected to be 14 mm, with a 1.5 mm heat extraction plate. This gradient zone configuration provided the geometric basis for the AADSF thermal model. Each furnace component was represented, along with the cartridge, ampoule, and sample material. The cartridge was positioned in the AADSF with the sample approximately centered in the gradient zone. The thermal model geometry corresponds to this assumed cartridge position.

Using the CAD program, each region representing a component or gas filled cavity was subdivided to better control meshing operations. When resistance-capacitance networks are defined by computing the thermal resistances between finite element centroids, local numerical errors result in the neighborhood of unstructured or nonrectangular mesh elements. Additional CAD based premeshing operations minimized the number of nonrectangular elements, and ensured that unavoidable nonrectangular elements occurred only in noncritical areas of the model. The thermal model geometry and computational mesh are shown in Figure 4.

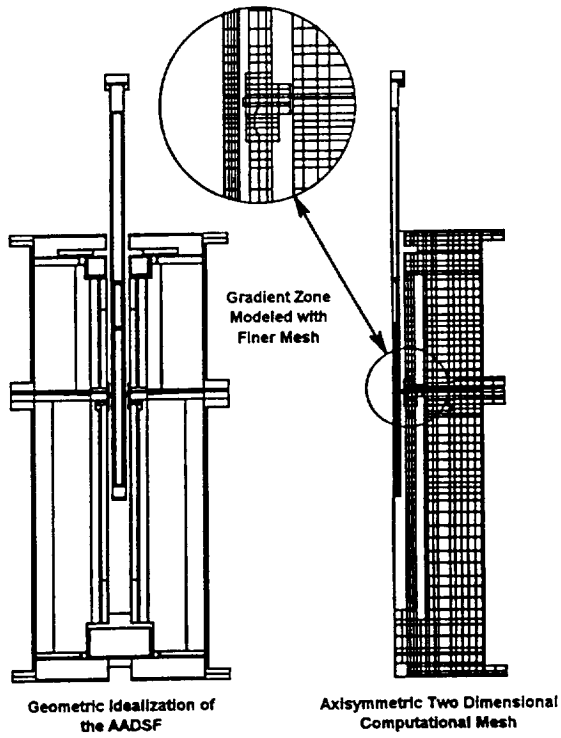

Figure 4: AADSF Thermal Model Geometry and Mesh

The CAD description of model geometry was imported into PATRAN™, which was then used to generate the detailed computational mesh. This mesh consists principally of rectangular elements, but includes some nonrectangular quadrilateral, triangular, and line elements. PATRAN™ was also used to generate

boundary conditions and material property assignments. The resulting finite element mesh was translated to a resistance-capacitance network in SINDA format. The SINDA input file resulting from this operation contained a complete description of the thermal conduction portion of the problem, but lacked material property values and radiation heat transfer modeling for cavities internal to the furnace.

Radiation conductance networks were computed for all gas filled voids inside the furnace. Such cavities include the annular regions separating the heater cores and primary insulation, the cartridge and furnace bore, and the sample/ampoule and cartridge tube. During mesh development, PATRAN™ was used to generate line elements on the surfaces of these regions. These elements provided a convenient geometric basis from which to construct thermal radiation models. Engineering judgment and a literature review [3, 4, 5] led to best estimates for the total hemispherical emissivity of the various radiating surfaces at furnace operational temperatures. These emissivity data completed the model description for computation of the thermal radiation conductance networks.

The Net Energy Verification and Determination Analyzer (NEVADA™) program was used to compute diffuse gray body solutions for the radiation conductance networks. View factors were statistically integrated using the Monte Carlo method. A total of 50,000 rays were randomly generated from each surface. The view factors were numerically integrated by counting the intersections of these rays with other surfaces in the model. With 50,000 rays, view factors as small as 0.01 are accurate to ±10% with 95% confidence [6]. The error bands decrease for larger view factors. Once the view factors were computed, gray body solutions were obtained with the Gebhart solver [7] included with NEVADA™ and translated to SINDA format.

Thermal conductivity data remained to be added to the AADSF thermal model. A literature review [3, 4, 5, 8, 9] resulted in arrays of temperature dependent thermal conductivity data. Addition of the radiation solutions and material data completed the AADSF thermal model description. The resulting model contained 2,150 nodes and 12,166 conductances interconnecting these nodes. Radiation modeling accounted for 68% of the conductors.

Although the AADSF thermal model description was essentially complete at this point, it was not ready for use as a parametric analysis tool. A proportional integrating control algorithm was added to the model to automatically adjust power to achieve the desired heater set point temperatures during iterative steady state solutions. On each iteration, the controller computes power adjustments from the set point error and the change in error since the previous iteration. Code was also added to permit specification of set point temperatures, material properties, and heat extraction plate thickness without requiring repetitive preprocessing. With these enhancements, the AADSF thermal model became a useful tool for parametric analysis.

Two major limitations apply to the AADSF thermal model. First, the model simulates only steady state conditions. Transient analysis was not needed to support the design effort. Second, since the AADSF thermal model is based on the differential equation of heat conduction, only results derivable from temperatures and heat fluxes can be computed. Convection and diffusion effects within the liquid portion of the sample cannot be simulated with this model.

Thermal Analysis and Application to Design

The AADSF thermal model served two main purposes. First it served as a parametric design analysis tool. The model was used to characterize AADSF gradient performance as a function of operating temperature and gradient zone design variables, including gradient zone insulation material and heat extraction plate configuration. The calculated peak axial temperature gradient induced in a quartz rod provided an analytical measure of gradient performance. The furnace model was also used to predict AADSF performance for the USMP-2 experiment.

Over 270 simulations were performed for the parametric analysis. For all cases, the thermal conductivity of quartz was used to represent the sample. In effect, this modeled a uniform quartz rod within the metallic cartridge, and provided a means of comparing thermal model predictions with performance goals and test data. Five parameters were varied in the study: (1) hot zone operating temperature - from 400°C to 1200°C, (2) cold zone control mode - isothermal or floating, (3) heat extraction plate material - Inconel 718 or pure platinum, (4) heat extraction plate thickness - ranging from zero to 3 mm, and (5) gradient zone insulation material - dense alumina, AL-30™, or FBD™.

When considering high thermal gradient operations, two bounding cold zone operational conditions are of interest. These two conditions are: (1) isothermal cold zone - the cold main and cold guard heaters are commanded to the same temperature, and (2) floating cold zone - the cold zone idles at minimum power with the cold guard heater temperature below that of the cold main. Isothermal cold zone operation requires significant power to the cold guard heater. Floating cold zone operation requires more heat from the booster heater for any given hot zone temperature, but typically results in

slightly less overall furnace power consumption. For true floating cold zone operation, the cold main and cold guard heaters would consume zero power. However a minimal power level, equivalent to one ampere to each heater, was applied for this analysis. This provided better estimates of minimum controllable cold zone temperatures for non-isothermal operation, and had a conservative effect on gradient performance predictions. Analysis clearly showed that, at the expense of cold zone isothermality, floating cold zone operation significantly increases the gradient capability of the AADSF.

For each steady state simulation, a converged solution was achieved using a successive over-relaxation method [10] to solve for all nodal temperatures. The solutions were not considered converged unless two criteria were met: (1) all nodal temperatures vary by less than 0.001°C between successive iterations, and (2) the net system energy imbalance was less than 1%. For each of 270 cases, the nodal temperature profile was computed. Results of specific interest, such as heater power requirements, cold zone temperatures, and peak axial quartz rod temperature gradients were computed.

The AADSF thermal model was run for five different hot zone temperatures ranging from 400°C to 1200°C in 200°C increments. An isothermal hot zone was simulated by commanding the hot guard, hot main, and booster heaters to the same set point temperature, and the peak axial temperature gradient induced in a quartz rod was computed. In general, larger gradients were produced at higher hot zone temperatures. The greater temperature difference between the hot zone and the cooling system allows larger temperature drops across the gradient zone to be developed, and thus larger gradients are produced. Gradient performance is further augmented at higher temperatures because of enhanced radiation heat transfer. Higher temperatures produce greater thermal radiation conductance, which results in sample temperature variations that correspond more directly with the steep thermal gradients of the furnace bore.

Both isothermal and floating cold zone operational modes were considered in this parametric analysis. Figure 5 plots the predicted axial gradient induced in a quartz rod versus hot zone temperature for a 1.5 mm Inconel 718 heat extraction plate and AL-30™ gradient zone insulation. The thermal model indicates that floating cold zone operation can more than double the AADSF gradient capability. For hot zone operation at 1100°C, a gradient in excess of 125°C/cm is predicted. Isothermal operation produces only 61°C/cm, short of the 100°C/cm goal. These results indicate that the first flight gradient objectives require operating the AADSF

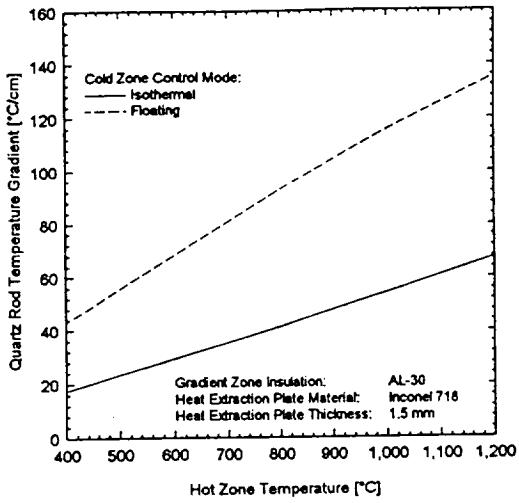

Figure 5: AADSF Gradient Performance versus Cold Zone Control Mode

with the cold guard heater commanded to a lower temperature than the cold main heater.

The parametric analysis considered two candidate high temperature materials for the heat extraction plate: platinum and Inconel 718. Figure 6 plots the predicted axial gradient induced in a quartz rod versus the hot zone temperature for a 1.5 mm heat extraction plate and AL-30™ gradient zone insulation, for both controlled and floating cold zone operation. For isothermal cold zone operation, a platinum plate significantly

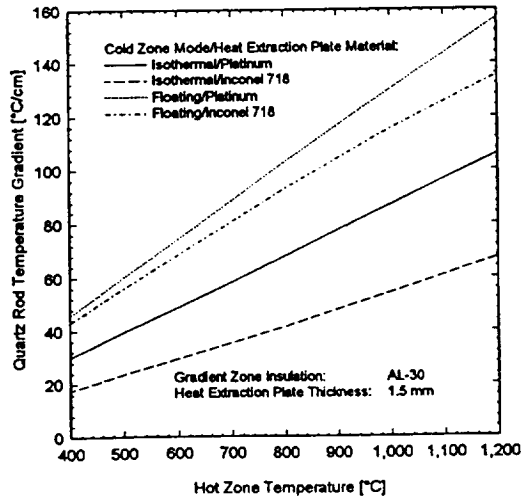

Figure 6: AADSF Gradient Performance versus Heat Extraction Plate Material and Cold Zone Control Mode

improves gradient performance, but still fails to meet the 100°C/cm required gradient for a hot zone at 1100°C. For floating cold zone operation, the platinum heat extraction plate results in somewhat higher gradients than an Inconel 718 plate, although both materials produce gradients in excess of the 100°C/cm design goal. As the hot zone temperature increases, the gradient performance gains that can be achieved with a platinum plate become more pronounced for both cold zone control modes. Since the USMP-2 experiment will be operated with the cold guard heater temperature below that of the cold main, Inconel 718 was selected for the heat extraction plate, because it met the gradient goal at a lower cost. Future AADSF experiments, if intended for high gradient and high temperature operation (above 1150°C), or if cold zone isothermality is more critical, may employ platinum heat extraction plates.

A range of candidate thicknesses were considered for the heat extraction plate in the design analysis: from zero to 3 mm in 0.75 mm increments. Figure 7 plots the predicted axial gradient induced in a quartz

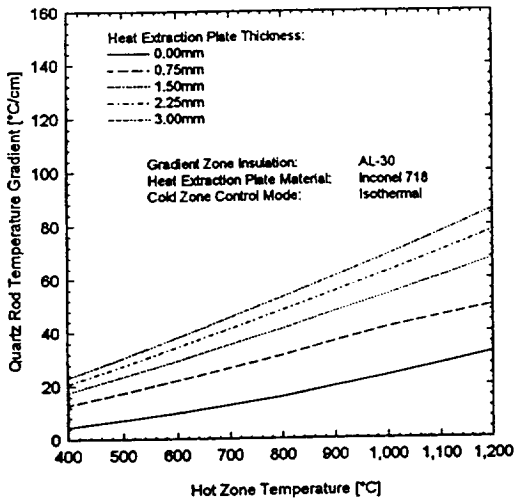

Figure 7: AADSF Gradient Performance versus Heat Extraction Plate Thickness for Isothermal Cold Zone Operational Mode

rod versus the hot zone temperature for isothermal cold zone operation, for the furnace equipped with an Inconel 718 heat extraction plate and AL-30™ gradient zone insulation. Although the 100°C/cm goal is not met, these results show that the heat extraction plate thickness can have a profound influence on gradient performance. Figure 8 plots the same results for floating cold zone operation. These results indicate that the 100°C/cm gradient goal is met for a hot zone operating at 1100°C without a heat extraction plate. The thermal

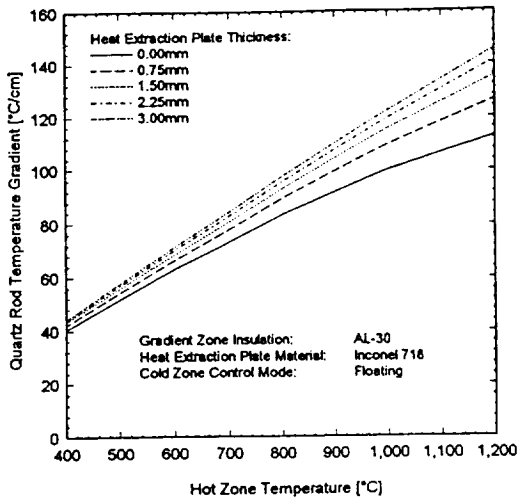

Figure 8: AADSF Gradient Performance versus Heat Extraction Plate Thickness for Floating Cold Zone Operational Mode

model shows that for floating cold zone operation, gradient performance is somewhat less sensitive to the heat extraction plate thicknesses than for isothermal cold zone operation. During floating cold zone operation, the cold guard heater operates at a lower temperature than the cold main heater. The temperature drop between these heaters provides an effective means of conducting hot zone heat transferred across the gradient zone to the cold zone end support structure. In the presence of this thermal path, the heat extraction plate thickness becomes less important with respect to gradient performance. However, at higher operating temperatures, the thermal conductivity simultaneously increases for the metallic heat extraction plate and decreases for the beryllia heater core materials, so an increase in heat extraction plate thickness produces more pronounced gradient performance gains.

Three candidate materials were considered for the gradient zone insulation: AL-30™, FBD™, and dense alumina. AL-30™ exhibits the best insulating properties, and dense alumina has the greatest mechanical strength. Figure 9 plots the predicted axial gradient induced in a quartz rod versus hot zone temperature for a 1.5 mm Inconel 718 heat extraction plate and floating cold zone operation. For a hot zone at 1100°C, AL-30™ and FBD™ both meet the 100°C/cm gradient goal, while dense alumina produces a gradient of only 52°C/cm. AL-30™ gradient zone insulation produces only slightly larger gradients than FBD™, despite its significantly lower thermal conductivity. This is due to heat conduction through the metallic insert that mechanically connects the gradient zone and heater cores

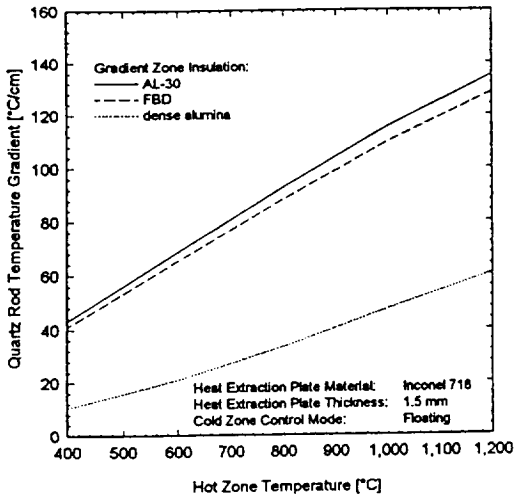

Figure 9: AADSF Gradient Performance versus Gradient Zone Insulation Material

to the furnace structure through the heat extraction plate. This insert provides a conduction path parallel to the gradient zone insulation, and renders the AADSF gradient performance relatively insensitive to the gradient zone insulation thermal conductivity values comparable to AL-30™ and FBD™. AL-30™ was chosen over the FBD™ material primarily because FBD™ principally contains zirconia, which becomes electrically conductive at high temperatures. This electrical conductivity could produce unwanted coupling between the resistive heater elements and their control thermocouples.

Performance Predictions for First Flight Configuration

Once the gradient zone was defined with AL-30™ insulation and a 1.5 mm Inconel 718 heat extraction plate, the AADSF thermal model was used to predict furnace performance for the USMP-2 experiment. Three cases were considered: (1) maximum hot zone and cold zone temperature, (2) maximum hot zone temperature and maximum gradient, and (3) USMP-2 experiment conditions.

The first case simulated maximum temperature operation in all heated zones with the hot zone at 1150°C and the cold zone at 850°C. The second case simultaneously simulated 1150°C maximum hot zone temperature and maximum gradient conditions. These two cases were analyzed to check heater power requirements against design heat dissipation limits. For both cases, the cartridge was assumed to contain a quartz rod rather than a sample/ampoule assembly. The cold main heater was predicted to float over its set point temperature for both cases. Set point errors of 1.6°C and 41.0°C were predicted for 850°C and 600°C cold zones, respectively. For the second case, a peak axial temperature gradient of 105°C/cm was predicted for the quartz rod. Table 2 lists the predicted heater power requirements. No power exceedances resulted from comparing the heat dissipated within the cores to the design limits. The results also indicate hot guard and hot main power requirements to be largely independent of cold zone temperature. However, reducing the cold zone set point from 850°C to 600°C significantly increased booster heater power demand.

Design		Thermal Analysis Results			
		1150/850°C Hot/Cold Zone		1150/600°C Hot/Cold Zone	
Heater Design-nation	Core Power Limit (Watts)	Core Power (Watts)	Total Power (Watts)	Core Power (Watts)	Total Power (Watts)
Hot Guard	320	228.5	249.8	227.4	248.6
Hot Main	930	159.9	173	164.9	178.4
Booster	275	117.5	164.2	149.1	208.4
Cold Main	130	0	0	0	0
Cold Guard	195	165.3	188.9	64.1	74
Total		671.2	775.9	605.5	709.4

Table 2: Predicted AADSF Power Performance at Design Temperature Limits

The third analysis case simulated AADSF performance for the USMP-2 experiment. For this simulation, all three hot zone heaters were commanded to 850°C, the cold main heater to 350°C, and the cold guard heater to 325°C. Table 3 lists the predicted heater power requirements for this operational condition. The results indicate the furnace should operate within its design power limits for the USMP-2 experiment. All five heaters were predicted to be powered and to operate without set point errors, indicating that active thermal control to these temperatures is possible for all five heated zones. Figure 10 illustrates the predicted axial temperature and temperature gradient profile through the sample. For this analysis, a representative melting temperature of 700°C was assumed. A sudden sample thermal conductivity change at the solidification temperature provided a simple means of representing the phase change at the interface. Actually, the thermophysical behavior of the USMP-2 sample material is considerably more complex. During processing, the

Design		Thermal Analysis Results	
Heater Designation	Core Power Limit (Watts)	850°C Hot Zone and 350/325°C Cold Main/Guard	
		Core Power (Watts)	Total Power (Watts)
Hot Guard	320	179.4	197
Hot Main	930	98.9	107.3
Booster	275	104.6	146.8
Cold Main	130	7.2	8.5
Cold Guard	195	8.7	10.2
Total		398.8	469.8

Table 3: Predicted USMP-2 AADSF Steady State Power Performance

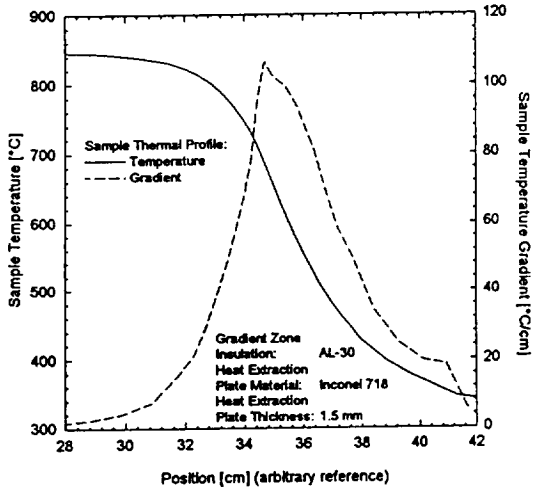

Figure 10: Predicted Sample Axial Temperature and Thermal Gradient Profile for the USMP-2 Experiment

sample melt becomes enriched with solute near the interface, resulting in compositional variations that cause the solidification temperature to change. The results in Figure 10 show a peak axial gradient in the sample of 106°C/cm. The location of the peak gradient corresponds closely to the 700°C melting point in the sample.

Comparison to Test

Steady state heater power predictions obtained from the AADSF thermal model have been compared to data obtained during ground testing. Power predictions provide the most effective means of assessing the predictive capabilities of this model, for two reasons. First, an understanding of power requirements is fundamental to the furnace design process. Second, a reliable representation of the thermal paths throughout the furnace would be indicated by accurate total and individual heater power predictions. With reliable power predictions, the model can be used to evaluate the feasibility of various experimental scenarios. Heater power can be evaluated against design power limits, and uncontrollable set point temperature combinations can be avoided.

Figures 11 and 12 compare predicted and measured steady state heater power for maximum power and maximum gradient operation, respectively. The results in these figures do not quite match the data in Table 2, because a customized empty-bore version of the model was used to better match the test conditions.

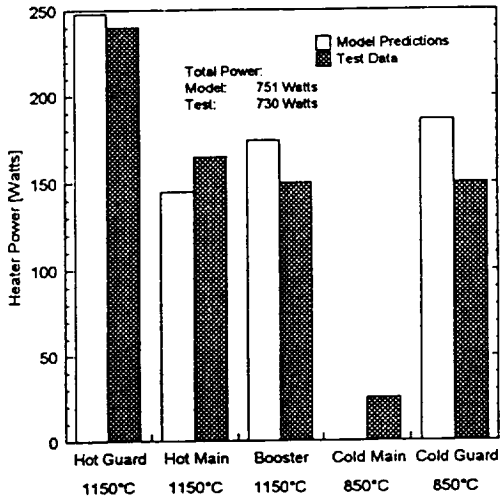

Figure 11: Predicted versus Measured Power for Maximum Hot Zone and Cold Zone Temperature

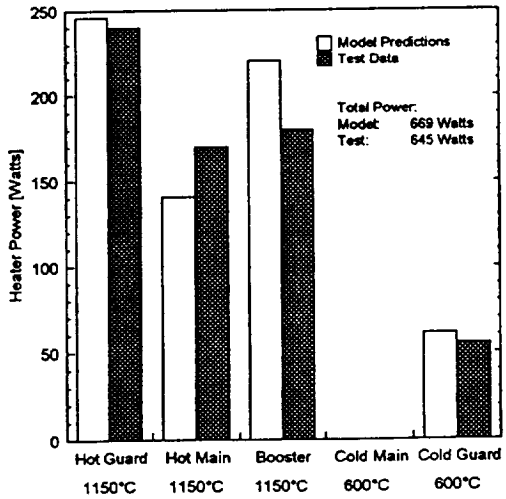

Figure 12: Predicted versus Measured Power for Maximum Hot Zone Temperature and Maximum Gradient

Predicted and measured distributions are similar, with predicted total power less than 5% higher than measured values. For the high gradient condition, the model predicted the cold main heater to operate 49°C above its 600°C set point. In the test, the steady state cold main temperature was 640°C.

Figure 13 compares predicted and measured power data for conditions representative of the USMP-2 experiment. The predicted and measured power distribution are quite similar, with predicted total power exceeding measured power by 8%. In Figure 13, the model more accurately predicts the power distribution than the empty-bore version shown in Figures 11 and 12. This is attributed to natural convection in the furnace bore during ground testing. The presence of the cartridge suppresses this convection during testing. Since the model includes no bore convection effects, predictions should correlate more closely to measurements for cartridge-in-bore conditions than for empty-bore conditions.

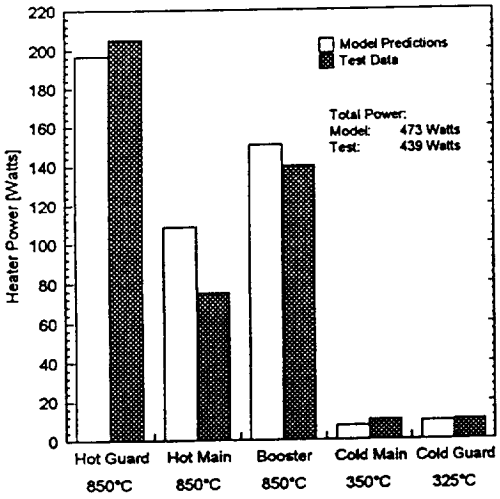

Figure 13: Predicted versus Measured Power for First Flight Conditions

Figure 14 compares measured and predicted temperature profiles within the cartridge. The test was performed with an alumina rod instrumented with four thermocouples, mounted inside a cartridge. Alumina thermal conductivity values were assigned to the region representing the sample in the model to better simulate this test condition. Figure 14 shows two presentations of the test data: (1) the thermocouple temperature closest to the cold end of the alumina rod recorded throughout cartridge translation, and (2) four individual temperature measurements taken at the end of translation. The temperature distribution predicted with the thermal model agrees well with measurements, although the model conservatively under-predicts the temperature gradient.

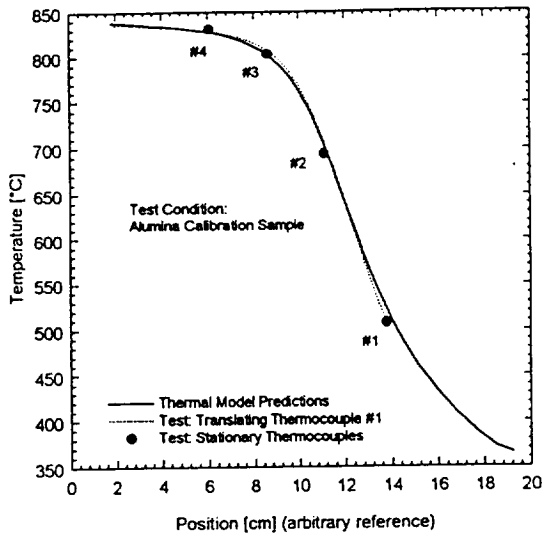

Figure 14: Predicted versus Measured Temperature for Calibration Sample and USMP-2 Temperatures

Conclusions

Thermal modeling proved to be an effective design tool during development of the AADSF. A thermal model was specifically developed to perform parametric analysis and used to characterize how the gradient zone design affects the thermal performance of the furnace. The results of the parametric analysis were used to select a gradient zone configuration to fulfill the requirements of the USMP-2 experiment. Furthermore, furnace characterization was achieved in far less time and expense with the thermal model than would be required to build a prototype and run an equivalent series of characterization tests.

Design analysis of the AADSF system predicting successful USMP-2 performance was later verified during tests conducted at Marshall Space Flight Center. Overall, the results obtained from the AADSF model compared well to measurements taken during tests. Steady state heater power requirements and temperature measurements obtained with a quartz rod instrumented with thermocouples were often within a few percent of predictions obtained with the thermal model. The apparent accuracy of the model is attributed largely to thorough handling of thermal radiation and temperature dependent material properties.

The high degree of flexibility built into the AADSF thermal model resulted in its success as a

parametric analysis and design tool. Code was added to permit user specification of design parameters such as the temperature dependent component thermal conductivity data or the heat extraction plate thickness. More importantly, code was added to automatically adjust heater powers to achieve the specified set point temperatures. Without this numerical heater control, heater powers would have to be specified and adjusted based on resulting temperatures, a process that would have rendered parametric design analysis impractical.

Several future expansions and uses for the AADSF thermal model are suggested by this work. With a thorough set of furnace characterization test data, the thermal model could be fine tuned to enhance its predictive capabilities. The model could be upgraded to transient capability and used to develop experiment timelines and fine tune heater control algorithms. The model could also aid in detailed analysis of crystal growth within the ampoule by providing realistic thermal boundary conditions at the furnace bore or cartridge wall. Because the AADSF thermal model is portable, it is available to the investigator to help develop effective crystal growth experiments. The model can be used to assess a large number of processing profiles before performing actual experiments, thereby saving valuable laboratory resources and experiment development time.

Acknowledgment

The Advanced Automated Directional Solidification Furnace (AADSF) was built by Teledyne Brown Engineering under contracts with the NASA Marshall Space Flight Center. The authors express appreciation to the project scientist, Dr. Sandor L. Lehoczky, and the NASA project manager, Mr. Fred Reeves. Without their hard work and commitment to microgravity science neither this paper nor the AADSF flight system would exist.

References

1. George C. Marshall Space Flight Center, AADSF End Item Specification, MSFC-SPEC-1196 A, 1987.

2. Lehoczky, S. L., Szofran, F. R., and Martin, B. G.: NASA CR-161598, Marshall Space Flight Center, Huntsville, AL, 1980.

3. Genium Publishing Corporation, Heat Transfer Databook, Schenectady, NY, 1984.

4. Westinghouse Astronuclear Laboratory, NERVA Program Materials Data Book, 1967.

5. Oak Ridge National Laboratory, Delivery of Data Base Information for MAPTIS/High Temperature Materials, 1988.

6. NEVADA Software Package User's Manual, Turner Associates Consultants, Incline Village, NV, 1988.

7. Gebhart, B. "Unified Treatment of Thermal Radiation Processes - Gray, Diffuse Radiators and Absorbers," ASME Paper 57-A-34, 1957.

8. Zircar Products, Inc., Technical Data Bulletin No. ZPI-212, Florida, NY, 1984.

9. MIL-HDBK-5E, Metallic Materials and Elements for Aerospace Vehicle Structures, US Department of Defense, 1987.

10. SINDA Users Manual, Network Analysis Associates, Fountain Valley, CA, 1992.